

## Development of supercritical motion and internal jumps within lock-release radial currents and draining flows

Edward W. G. Skevington <sup>1</sup>, Andrew J. Hogg <sup>1,\*</sup> and Marius Ungarish <sup>2</sup>

<sup>1</sup>*School of Mathematics, University of Bristol, Bristol BS8 1UG, United Kingdom*

<sup>2</sup>*Department of Computer Science, Technion, Israel Institute of Technology, Haifa 32000, Israel*



(Received 26 February 2021; accepted 4 June 2021; published 24 June 2021)

The unsteady radial flow of a relatively dense fluid released from an axisymmetric lock is analyzed when it freely drains over an edge and when it generates a gravity current propagating over a horizontal surface. In both situations when modeled using the shallow water equations, despite initiation from rest within a lock, the flow thins, accelerates, and becomes supercritical in a region close to the symmetry axis. For free drainage, this alters the outflow, while for radial gravity currents, it leads to the formation of an internal jump connecting rapidly moving fluid to more tranquil flow at the front. Both scenarios share the same supercritical flow structure, which is related to their initiation from lock-release conditions and is a function of axisymmetry; the phenomenon is not found in analogous two-dimensional flows. Through analysis and numerical integration of the governing equations, the common onset and consequences of supercriticality are revealed in both flows, as well as, the progression of the fluid motions to self-similar states that develop at late times.

DOI: [10.1103/PhysRevFluids.6.063803](https://doi.org/10.1103/PhysRevFluids.6.063803)

### I. INTRODUCTION

Axisymmetric gravity currents—the predominantly horizontal, radial flow of relatively dense fluid through less dense environments—are ubiquitous in natural and industrial applications [1]. Large-scale examples include the dispersion at ground level of dense and potentially hazardous gases [2–4] and the development of umbrella clouds of volcanic ash in the atmosphere [5–7]. The instantaneous release of dense fluid and its axisymmetric propagation is therefore an important canonical problem that has been researched through laboratory experiments, modeling, and numerical simulations (see, for example, [8–10]).

Compositionally driven gravity currents that propagate over underlying horizontal boundaries at sufficiently high Reynolds numbers that the viscous effects are negligible (at least during the initial phases) flow as relatively thin layers. Thus the motion is governed by hydrostatic balance to leading order and the shallow water equations have been shown to represent accurately the ensuing dynamics, when coupled to a dynamic boundary condition at the moving front that accounts for nonhydrostatic motion as the less dense environmental fluid is displaced [11]. Within this modeling framework, radial flows generated by the instantaneous release of fluid from a lock evolve to a self-similar state [12,13]. There is, however, hitherto unexplained dynamics that arise during the initial adjustment. For example, [11] demonstrated that the fluid develops a rapidly moving, very thin layer at the rear of the current, which eventually leads to the formation of an internal jump (or ‘shock’), over which the velocity and height of the flow change discontinuously. This is peculiar

---

\*a.j.hogg@bristol.ac.uk

to axisymmetric releases; there is no shock formation in this way at early times for their two-dimensional (2D) counterparts [14].

A related flow is the unsteady drainage from a reservoir that occurs when the fluid is allowed to flow freely over an edge [15,16]. At relatively early times, the dynamics within the draining reservoir are similar to the development of a radial gravity current released from a lock into an otherwise quiescent ambient. Thus we anticipate the onset of a thin, rapidly moving layer, which could potentially lead to supercritical outflow. Once again, this effect is not observed in the 2D version of this problem (cf. [15]).

In this paper, we analyze the axisymmetric flow of relatively dense fluid released from rest in a circular cylindrical or annular reservoir by the abrupt removal of the confining lockgate. From these lock-release conditions, the flow propagates horizontally over a rigid boundary through otherwise quiescent fluid. We study two flow scenarios: in the first we examine free drainage over an edge (Sec. III), while in the second we investigate radial gravity currents (Sec. IV). These problems are linked because the radial geometry influences the development of the flow from the initial conditions, and our new contributions are to reveal the origins of unexplained features of the motion and to relate them to this initial evolution. We show that there is commonality between the two problems: the self-similar supercritical motion found as fluid drains freely over an edge is the same as the supercritical flow that develops within the lock of an axisymmetric gravity current and persists for an extended period. For both problems, our analysis reveals that radial spreading leads to the thinning of the initially quiescent fluid and the development of supercritical conditions (Sec. III). We reiterate that this is due to the radial geometry; it does not occur for 2D currents. Importantly our analysis reveals the origin of key features, namely, that radial, free-draining fluid over an edge develops supercritical flow internally (Sec. III) and that radial gravity currents develop a supercritical outflow from the reservoir, which leads to the formation of a shock as it connects with the slower motion close to the front (Sec. IV). Crucially, we use the new insights to explain the inception and subsequent behavior of the shock and to reveal how it moves within the flowing current and impacts the approach to the late-time, similarity state for the motion (Sec. IV).

Our methods combine high-resolution numerical simulations of the governing partial differential equations with analytical insights. We construct the flow solutions at early times using a perturbation expansion and at late times using similarity solutions, to which we elucidate the progressive flow adjustment.

The flows analyzed in this paper provide further instances of when radial dynamics differ in a nontrivial way from their 2D counterparts. Previously reported examples include radial gravity currents sustained by a constant flux [7], which do not tend to a self-similar state envisaged in [17]. Instead a more complex flow pattern develops in which there is a steady tail, connected to an unsteady frontal region, and this flow structure is inconsistent with a ‘global’ self-similar solution. Indeed for this flow, it leads to a different temporal dependence of the position of the front, which can nevertheless be deduced asymptotically [7]. The same flow structure is found in sustained radial currents through stratified environments [7], which led to the development of a new ‘hybrid’ model that couples the steady dynamics of the tail to an unsteady frontal region [18]; the latter is treated as spatially uniform and this permits a representation of the unsteady dynamics that is easy to compute. This hybrid approach was also extended to currents affected by Coriolis forces [19].

The paper is structured as follows. We first present the governing equations and boundary conditions for the flows and provide brief details of the numerical methods (Sec. II). We then analyze free draining from a cylindrical or annular reservoir, demonstrating the onset of supercritical flow and the establishment of a self-similar flow state (Sec. III). Interestingly it is only for cylindrical reservoirs that a supercritical, self-similar flow state may be established (Sec. III B) and we show that that it is dependent upon the precise initial conditions (Sec. III D). For annular reservoirs, in contrast, the late-time drainage always exhibits critical conditions at the outflow for which we derive a new similarity solution (Sec. III C)—although the transient dynamics are supercritical and the approach to the self-similar state may be very long-lived (Sec. III B). Radial gravity currents generated from lock-release conditions exhibit the same development of supercritical flow conditions at an interior

location, eventually leading to the development of a shock across which the dependent variables change discontinuously. We compute the motion of the shock and demonstrate how it affects the approach to the late-time self-similar solution (Sec. IV). Brief conclusions are given in Sec. V. The paper also includes an Appendix in which we provide some additional details of the new self-similar, radial draining solution from an annular lock.

## II. FORMULATION

We employ polar coordinates, centered on the axis of the confining reservoir, and model the axisymmetric evolution of the dimensionless height,  $h(r, t)$ , and radial velocity,  $u(r, t)$ , of the fluid layer. The reservoir initially confines a volume  $\pi\mathcal{V}$  of fluid; it is of dimensional radius,  $R$ , and in the case of an annular release, the dimensional inner radius is at  $Rr_i$ . Horizontal radial lengths are scaled by  $R$ , the depth of the fluid is scaled by  $H = \mathcal{V}/[R^2(1 - r_i^2)]$ , and times are scaled by  $R/(g'H)^{1/2}$ , in which the reduced gravity is  $g' = (\rho_1 - \rho_2)g/\rho_1$ , where  $g$  denotes the gravitational acceleration and  $\rho_1$  and  $\rho_2$  denote the densities of the intruding and ambient fluids, respectively ( $\rho_1 > \rho_2$ ). The motion is modeled on the assumption that the flow is shallow ( $(H/R)^2 \ll 1$ ), predominantly parallel to the underlying boundary, and so the pressure is hydrostatic to leading order. Furthermore, viscous effects are assumed negligible ( $[g'H^5]^{1/2}/[R\nu] \gg 1$ , where  $\nu$  denotes the kinematic viscosity) and then the dimensionless nonlinear shallow water equations are given by

$$\frac{\partial h}{\partial t} + \frac{1}{r} \frac{\partial}{\partial r}(ruh) = 0, \quad (1)$$

$$\frac{\partial u}{\partial t} + u \frac{\partial u}{\partial r} + \frac{\partial h}{\partial r} = 0, \quad (2)$$

which represent the conservation of mass and the balance of radial momentum, respectively (see [9]). These equations are applied within the dimensionless domain  $r_i < r < 1$  for free-draining flow or  $0 < r < r_N(t)$  for gravity current flows, where  $r_N(t)$  denotes the position of the front. [For gravity currents we treat only releases from cylindrical reservoirs ( $r_i = 0$ ).] We enforce vanishing velocity at the inner boundary  $u(r_i, t) = 0$ , noting that if  $r_i = 0$ , then this condition arises due to the radial symmetry of the motion. The initial conditions, unless stated otherwise, are those of lock release, given by  $u(r, 0) = 0$  and  $h(r, 0) = 1$  for  $r_i < r < 1$  and vanishing elsewhere. The configuration of the flows is depicted in Fig. 1.

It is insightful to interpret the motion in terms of the characteristics of the governing equations, (1) and (2), which are given by

$$\frac{d}{dt}(u \pm 2h^{1/2}) = \mp \frac{uh^{1/2}}{r} \quad \text{on} \quad \frac{dr}{dt} = u \pm h^{1/2}. \quad (3)$$

It is convenient for the discussion that follows to introduce the characteristic functions  $\alpha = u + 2h^{1/2}$  and  $\beta = u - 2h^{1/2}$ .

The free-draining boundary condition demands that the flow is at least critical at the outflow, which is given by

$$u \geq h^{1/2} \quad \text{at} \quad r = 1. \quad (4)$$

The model equations for free-draining flow over an edge [(1), (2), and (4)] are identical to those analyzed in [16], except that in [16] criticality was demanded at the outflow ( $u = h^{1/2}$ ). The boundary condition used in [16] was inspired by the draining flow in a rectangular reservoir [15], and in that geometry with the absence of curvature terms, the outflow is critical all the time. However, when curvature terms are present, a more subtle balance develops, and this effect has been missed in the previous investigations. In what follows we demonstrate that imposing criticality on the system is overprescriptive (see Sec. III); formally there is no solution with criticality imposed and attempts to simulate the system numerically exhibit artifacts, as the interior dynamics are inconsistent with the boundary condition. Instead in this study, we impose that the flow is at least

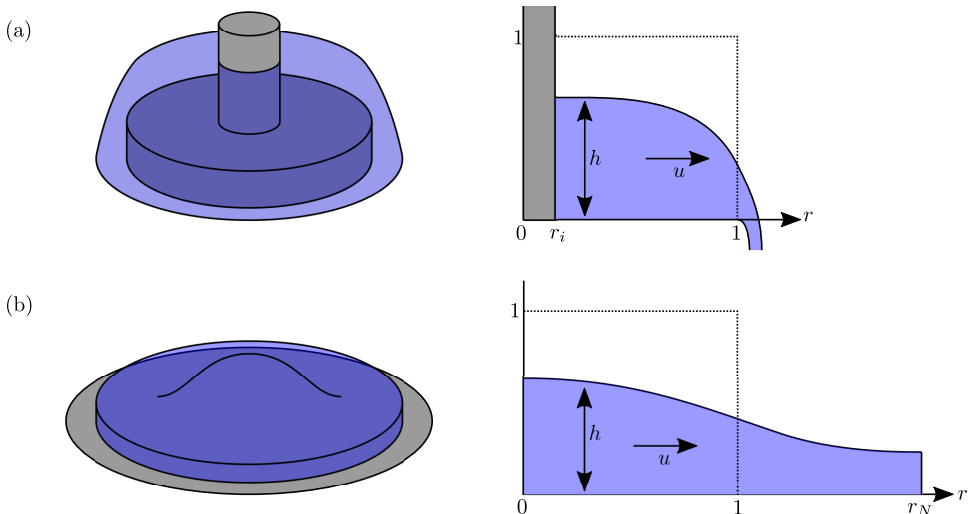


FIG. 1. The configuration of (a) draining flows and (b) gravity currents. Note that the vertical scales are exaggerated; the flows under consideration are assumed to be shallow.

critical, and as shown below, this apparently small change removes the incompatibility and yields supercritical dynamics. We also show that this effect is surprisingly nonlocal: the presence of an inner radius  $r_i > 0$  influences significantly the critical/supercritical behavior at  $r = 1$ , including in the self-similar phase; the qualitative effects are shown to be independent of the value of  $r_i$ .

Alternatively, for gravity current flow, we enforce a dynamic condition at the front [20,21], which may be written as

$$\frac{dr_N}{dt} = u = \text{Fr}h^{1/2} \quad \text{at} \quad r = r_N(t), \quad (5)$$

where the Froude number at the front,  $\text{Fr}$ , is a function of the ratio of the densities,  $\rho_1/\rho_2$ . For motion through a relatively deep ambient fluid, it may be shown theoretically that  $\text{Fr} = (2\rho_1/\rho_2)^{1/2}$  [20,21], while for Boussinesq regimes [ $(\rho_1 - \rho_2)/\rho_1 \ll 1$ ], it has been established experimentally that  $\text{Fr} = 1.2$  [22]. In the analysis in Sec. IV we impose various values of the frontal Froude number,  $\text{Fr} \geq 1$ , and demonstrate an important difference in the evolution depending on whether  $\text{Fr}$  is less than or greater than  $\sqrt{2}$ . The model for radial gravity currents [(1), (2), and (5)] is identical to what has been investigated by many previous researchers (see, for example, [17,12,11]) and the novelty of our contribution lies in the interpretation of the dynamics following initiation, in particular, the emergence of internal jumps (shocks) and the late-time behavior.

We comment that an equivalent framework arises for modeling the propagation of an axisymmetric release of fluid that is less dense than its surroundings, propagating along an upper horizontal boundary. Continuing to denote the intruding density  $\rho_1$  and the deep ambient  $\rho_2$  (but now with  $\rho_1 < \rho_2$ ), we define the reduced gravity by  $g' = (\rho_2 - \rho_1)g/\rho_1$  and derive the dimensionless governing equations, (1) and (2), for the conservation of mass and momentum. The dynamic boundary condition boundary, (5), is still given by  $\text{Fr} = (2\rho_1/\rho_2)^{1/2}$  [20], and thus  $\text{Fr} < \sqrt{2}$  for these buoyant currents.

The governing equations, (1) and (2), are integrated numerically. This is done by rewriting the equations in terms of the numerical variable  $Q = [(r_N - r_i)rh, (r_N - r_i)^2 r \tilde{u}h]^T$  and rescaled spatial coordinate,  $\tilde{r} = (r - r_i)/(r_N - r_i)$ , where  $\tilde{u} = u - \tilde{r}dr_N/dt$ , which is the axisymmetric equivalent of the transformation of the 2D shallow water equations presented in [23]. The numerical scheme used is the central upwind scheme presented in [24]. This is a finite-volume scheme which requires reconstruction in each cell; for this purpose we reconstruct in the variable  $S = [h, r \tilde{u}h]^T$ , using the

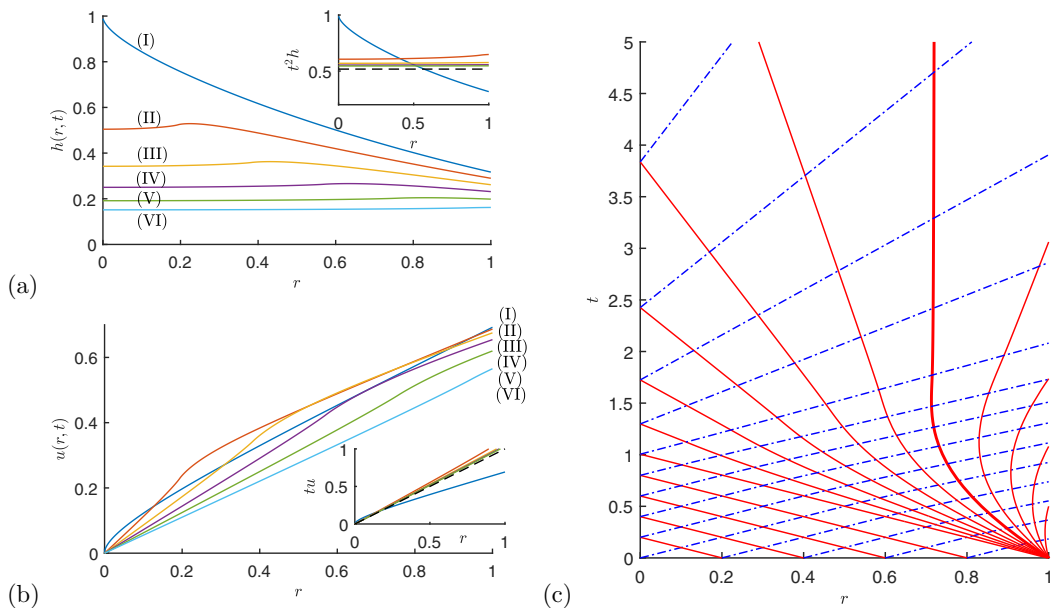


FIG. 2. (a) Height,  $h(r, t)$ , and (b) velocity,  $u(r, t)$ , fields as functions of the radial distance from lock-release initial conditions, with  $r_i = 0$  at  $t = 1, 1.2, 1.4, 1.6, 1.8,$  and  $2$  denoted (I)–(VI), respectively (solid lines). Insets: Plots of (a)  $t^2 h(r, t)$  and (b)  $tu(r, t)$  as functions of the time at  $t = 1, 2, 3, 4,$  and  $5$ , (solid lines) along with the similarity solutions, (16) (dashed lines). (c) The associated characteristic plane showing  $\alpha$  characteristics (dot-dashed blue lines) and  $\beta$  characteristics (solid red lines). Note that there is a  $\beta$  characteristic which lies along  $r = 0.72$  for  $t > 1.4$  (thick red line), which implies that critical conditions ( $u = h^{1/2}$ ) on this curve prevail, together with supercritical conditions for  $r > 0.72$ .

modified minmod limiter and a transformation of the reconstructed gradient in  $h$  into one for  $Q_1$  [25,26]. The boundary condition, (4), is selected by evaluating the values in the cell adjacent to the domain end; if it is subcritical, then criticality is imposed, whereas if it is supercritical, then no algebraic boundary condition is applied. The system of equations for the boundary values is closed by imposing the characteristic equations for the fields leaving the domain. This approach is identical to the technique proposed for test problem 6.1 in [23]. The conditions, (5), are implemented similarly, augmenting the algebraic conditions with the outgoing characteristic equation. For the boundary conditions, (4) and (5), the flux of  $Q$  through the boundaries is computed directly from the values at the boundaries. The simulations were performed at a resolution of at least 1000 cells.

### III. FREE DRAINING OVER AN EDGE

#### A. Cylindrical reservoir ( $r_i = 0$ )

We first focus on free draining from a circular reservoir ( $r_i = 0$ ), for which numerically computed profiles of the height and velocity fields are plotted in Figs. 2(a) and 2(b). We find that the initial phase of the motion corresponds to a collapse of the fluid layer adjacent to the edge, which progressively sets more of the fluid in the reservoir into motion. This initial motion corresponds to a fan of  $\beta$  characteristics centered on  $r = 1$  [Fig. 2(c)]. At very early times, this fan is similar to a dam break in Cartesian coordinates for which  $u = u_0 \equiv 2(1 + y)/3$  and  $h = h_0 \equiv (2 - y)^2/9$ , where  $y = (r - 1)/t$  [27], and thus within it, the  $\beta$  characteristics are initially straight lines emanating from  $r = 1$ . However, the characteristic curves are altered as time evolves, and in particular, the  $\beta$  characteristics from the origin  $y = 0$  (i.e., the edge of the lock,  $r = 1$ ) become curved. This is evident from the plot of  $\alpha$  and  $\beta$  families of characteristics [Fig. 2(c)]. Importantly, we note

that some of the  $\beta$  characteristics become no longer rearward propagating but, instead, propagate forwards and out of the domain. This change in the direction of  $\beta$  characteristics is straightforward to justify from the governing equations written in characteristic form, (3): since  $u$  and  $h$  are both positive, the rate of change of  $\beta$  on a characteristic is also positive and consequentially the characteristic velocity ( $dr/dt = u - \sqrt{h}$ ) also increases. Furthermore, we may explicitly compute the form of these characteristics when  $t \ll 1$  by writing

$$h = h_0(y) + th_1(y) + \dots \quad \text{and} \quad u = u_0(y) + tu_1(y) + \dots \quad (6)$$

We find  $h_1(y)$  and  $u_1(y)$  by substituting into the governing equations, (1) and (2), balancing at  $O(t)$ , and imposing  $u = 0$  and  $h = 1$  on  $y = -1$ , which corresponds to the rearmost  $\beta$  characteristic from the fan propagating into the quiescent reservoir. In this way we find that

$$h_1 = \frac{1}{9}(y-6)(2-y)^2 + \frac{7\sqrt{3}}{27}(2-y)^{5/2} \quad \text{and} \quad u_1 = \frac{5\sqrt{3}}{9}(2-y)^{3/2} - \frac{1}{3}(y-4)(y-2). \quad (7)$$

Then the  $\beta$  characteristics emanating from  $r = 1$  at  $t = 0$  are given by

$$r = 1 + \left(\frac{2+3\beta_0}{4}\right)t + \frac{3}{32}(2-\beta_0)^{3/2}(2-(2-\beta_0)^{1/2})t^2 + \dots, \quad (8)$$

where  $\beta_0$  labels each  $\beta$  characteristic from  $r = 1$  with  $-2 \leq \beta_0 \leq -2/3$ . Since the quadratic term in (8) is positive, it is therefore evident that the characteristic velocity is increased and that some  $\beta$  characteristics from the fan will leave the domain as depicted in Fig. 2(c).

That both  $\alpha$  and  $\beta$  families of characteristics propagate out of the domain is crucial. It implies that the outflow is supercritical  $u(1, t) > [h(1, t)]^{1/2}$  for at least some initial phase of the motion. We plot the evolution of the Froude number at the edge,  $F_o \equiv u(1, t)/[h(1, t)]^{1/2}$ , as a function of time [Fig. 3(a); curve (i)] and note that it is supercritical and increases to a maximum value before becoming constant throughout the motion ( $F_o = 1.39$ ) for  $t > 2.5$ . This means that at long times there is an interior  $\beta$  characteristic on which  $u = h^{1/2}$  and thus it does not leave the domain. This ‘critical’  $\beta$  characteristic is plotted in Fig. 2(c) and at long times lies along  $r = 1/1.39 = 0.72$  (see Sec. III C); it corresponds to the  $\beta$  characteristic for which  $\beta_0 = -1.18$ .

We may extend our series expansion, (6), for the height and velocities to include terms of  $O(t^2)$ , and in this way, we determine the Froude number at the outflow up to  $O(t^2)$ :

$$F_o \equiv \frac{u(1, t)}{[h(1, t)]^{1/2}} = 1 + \left(\frac{1}{2}\sqrt{6} - 1\right)t + \left(\frac{161}{12} - \frac{71}{12}\sqrt{6} + \frac{8}{3}\log\frac{3}{2}\right)t^2 + \dots \quad (9)$$

In Fig. 3 we see that this expression accurately captures the initial growth of the Froude number at the outflow as the flow within the reservoir becomes supercritical. We may also use our expansions to  $O(t^2)$  to evaluate the drainage volume flux at the outflow,  $q = u(1, t)h(1, t)$ ,

$$q = \frac{8}{27}(1 + (4\sqrt{6} - 10)t + \left(\frac{387}{2} - \frac{490}{6}\sqrt{6} + 16\log\frac{3}{2}\right)t^2 + \dots). \quad (10)$$

This expression for  $q$  is plotted along with the numerically computed flux from the integration of the governing partial differential equation [Fig. 3(b)]. We note that the asymptotic expression, (10), is accurate for  $t < 1.5$ , by which time the volume of fluid remaining within the reservoir has decreased to 28% of its initial value. The temporal behavior of the flux at later times is accurately predicted by the similarity solution derived below (Sec. III C).

## B. Annular reservoir ( $r_i > 0$ )

We also analyze the motion when the fluid is released from an annulus ( $r_i > 0$ ). Once again we plot the Froude number at the edge as a function of the time for various values of  $r_i$  [Fig. 3(a)]. We detect somewhat different behavior: from the lock-release initial conditions, the outflow becomes supercritical and the Froude number at the outflow rises to attain a maximum value. Thereafter, rather than maintaining a constant value as it does when  $r_i = 0$ , the Froude number decreases,

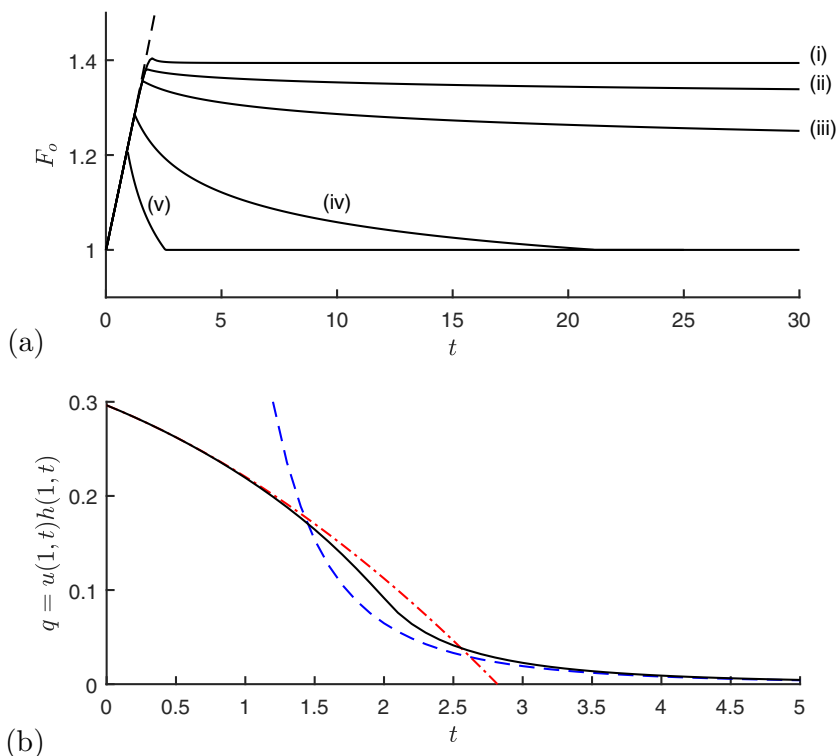


FIG. 3. (a) Froude number at the outflow,  $F_o$ , as a function of the time for (i)  $r_i = 0$ , (ii)  $r_i = \frac{1}{10}$ , (iii)  $r_i = \frac{1}{6}$ , (iv)  $r_i = \frac{1}{3}$ , and (v)  $r_i = \frac{1}{2}$  (solid lines). Also plotted is the asymptotic expression for  $F_o$  at early times (dashed line). (b) Outflow flux,  $q$ , as a function of the time (solid black line). Also plotted are the series expansion, (10), derived when  $t \ll 1$  (dot-dashed red line) and the similarity solution, (16), when  $t \gg 1$  (dashed blue line).

eventually reaching a time at which it has become critical, and subsequently the explicit condition of criticality at the outflow is enforced. We note further that the decay of the Froude number at the outflow is rather slow when  $r_i \ll 1$ . For example, cases (ii) and (iii) in Fig. 3(a), for which  $r_i = \frac{1}{10}$  and  $\frac{1}{6}$ , respectively, do attain critical conditions at the outflow but at times beyond those plotted. However, as shown below, the only long-term state for flows with  $r_i > 0$  is one with critical outflow conditions.

Figure 3(a) also reveals that during the initial phase of the motion when the Froude number at the outflow is rising, all simulations follow the same evolution given by (9). This arises because the effects of the no-flow condition at  $r = r_i$  are yet to influence the drainage outflow. For  $|1 - r_i| \ll 1$ , the simulated behavior departs from (9) by the arrival at the outflow of the  $\alpha$  characteristic that is generated at  $r = r_i$  by the rearmost  $\beta$  characteristic from the initial fan centered at  $r = 1$ . However, for  $r_i \ll 1$  the maximum Froude number at the outflow is attained slightly before this time. In Fig. 4 we plot the numerically computed arrival time at the outflow of the first  $\alpha$  characteristic initiated at the back wall by the arrival of the rearmost  $\beta$  characteristic from the initial fan as a function of the radius of the back wall,  $r_i$ . In other words, we integrate

$$\frac{dr_c}{dt} = u(r_c, t) + \sqrt{h(r_c, t)} \quad \text{subject to} \quad r_c(t_0) = r_i, \quad (11)$$

where  $t_0 = 1 - r_i$ , and we evaluate  $t_a$  such that  $r_c(t_a) = 1$ . We have also plotted in Fig. 4 the values at the selected annular radii plotted in Fig. 3 when the outflow Froude number reaches its maximum value. We note that there is a very close correspondence between these times. When  $|1 - r_i| \ll 1$ ,

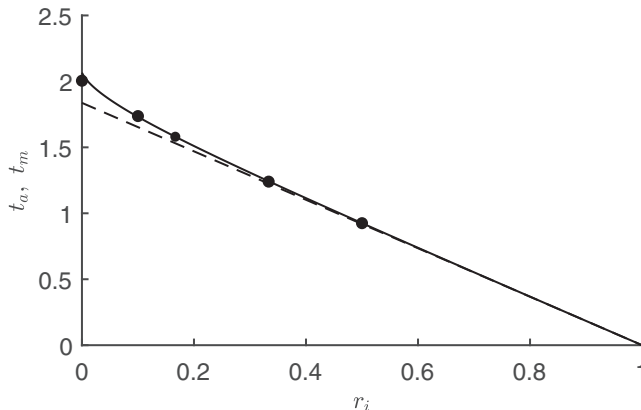


FIG. 4. The arrival time at the outflow,  $t_a$ , of the  $\alpha$  characteristic that is launched from the inner wall by the arrival of the rearmost  $\beta$  characteristic from the rarefaction fan as a function of the inner annular radius,  $r_i$  (solid line). Also plotted are points that correspond to the times at which the Froude number at the outflow is maximized,  $t_m$  [see Fig. 3(a)], and the asymptotic dependence of  $t_a$  when  $1 - r_i \ll 1$  given by (12) (dashed line).

we may use  $u_0$  and  $h_0$  to determine that

$$t_a = \left(\frac{3}{2}\right)^{3/2} (1 - r_i) + \dots, \quad (12)$$

and note that this quite accurately captures the arrival times for  $r_i > 0.3$ .

For practical purposes, we observe that the volume of fluid remaining in the reservoir monotonically decreases with time and that by  $t \approx 5$  it has decreased to less than 3% of its original value for all cases plotted in Fig. 3(a). Critical conditions at the outflow have only been attained in the case  $r_i = 0.5$  by this time and thus the return to criticality may not be physically important if  $r_i \ll 1$ , with the bulk of the drainage occurring as the transient supercritical flow.

### C. Self-similar behavior

Following [16], we seek a self-similar form for the motion when  $t \gg 1$  and the motion has become independent of the initial conditions. To this end we look for solutions of the form

$$u(r, t) = \frac{r}{t} V(r) \quad \text{and} \quad h(r, t) = \frac{r^2}{t^2} \frac{V(r)^2}{F(r)^2}, \quad (13)$$

where  $V(r)$  and  $F(r)$  are the similarity functions to be determined. Note that  $F(r) = u(r, t)/[h(r, t)]^{1/2}$  is the local Froude number. When substituted in (1) and (2), these give two coupled ODEs,

$$r \frac{dV}{dr} = -\frac{(V-1)(F^2-2)}{F^2-1}, \quad (14)$$

$$r \frac{dF}{dr} = \frac{F(F^2(V+1) + 2V - 4)}{2V(F^2-1)}, \quad (15)$$

which are subject to boundary conditions  $r_i V(r_i) = 0$  and  $F(1) \geq 1$ .

Substitution of  $s = \log r$  converts (14) and (15) into an autonomous system and we may plot trajectories in the  $(F, V)$  plane (Fig. 5). It is notable that the line  $F = 1$  is singular unless  $V = 1$  at the same value of  $r$ , in which case there are just two trajectories that pass through this point.

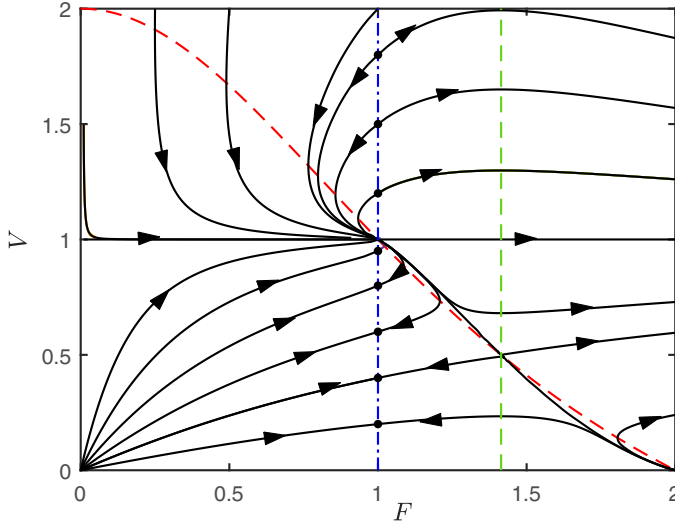


FIG. 5. Trajectories in the  $(F, V)$  phase plane, with arrows depicting the direction of evolution with increasing  $r$ . Also plotted are nullclines ( $dV/dr = 0$ , dashed green line;  $dF/dr = 0$ , dashed red line) and  $F = 1$  (dot-dashed blue line). Recall that  $V(r_i) = 0$  for  $r_i > 0$  and hence only the lower left quadrant is relevant for an annular reservoir.

### 1. Cylindrical reservoir ( $r_i = 0$ )

The case  $r_i = 0$  is special because the condition  $r_i V(r_i) = 0$  is automatically satisfied and because there is a family of solutions given by

$$V(r) = 1 \quad \text{and} \quad F(r) = F_o r, \quad (16)$$

where  $F_o$  is constant and  $F_o \geq 1$ . In terms of the original dependent variables, the solution is  $u = r/t$  and  $h = 1/(F_o^2 t^2)$ . If  $F_o = 1$ , then this similarity solution corresponds to that proposed by [16]. However, we find from our numerical simulations that the outflow remains supercritical with  $F_o = 1.39$  (see Fig. 3) and that this similarity solution is established after a relatively short time following release [see Figs. 2(c) and 3]. It was observed above that there is a  $\beta$  characteristic on which critical conditions are attained that remains within the domain. From the similarity solution, it is located at  $r = 1/F_o$  [see Fig. 2(c)].

Similarity solutions of the form of (13) are only defined up to an arbitrary temporal offset; replacing  $t$  with  $t + \tau$  would otherwise leave the solution unchanged. In general there is no ‘rigorous’ way to determine theoretically the temporal offset that would lead to the similarity solution, (13), most closely matching the computed numerical solutions. For practical purposes we equate the drainage flux,  $q$ , at  $t = 2$  to the similarity drainage flux including a temporal offset,  $1/[F_o^2(2 + \tau)^3]$ , and find that  $\tau = -0.218$ ; for  $t > 2$ , the subsequent difference between the numerically computed drainage flux and its similarity form with the temporal offset remains less than  $5 \times 10^{-3}$  and the relative difference less than  $6 \times 10^{-2}$ .

### 2. Annular reservoir ( $r_i > 0$ )

When  $r_i > 0$  the solution is rather different. We cannot construct a similarity solution of the form of (13) which is supercritical at the front because there are no trajectories in the  $(F, V)$  phase plane that pass from the inner wall boundary,  $V(r_i) = 0$ , to a supercritical state. Instead we can only find similarity solutions that are critical at the draining edge [ $F(1) = 1$ ] (see Fig. 6).

This therefore rationalizes the behavior reported in Sec. III B. The Froude number at the edge when  $r_i > 0$  initially reaches a supercritical state due to the initial evolution from lock-release

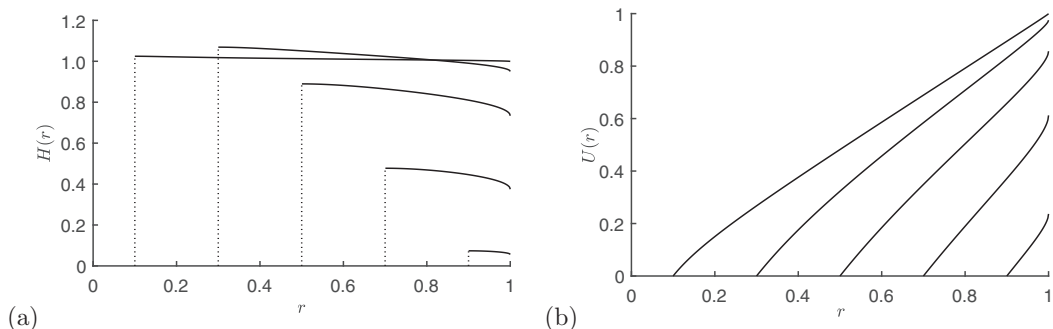


FIG. 6. Similarity solutions for (a)  $H(r) = (rV/F)^2$  and (b)  $U(r) = rV(r)$  as functions of the radial distance for  $r_i = 0.1, 0.3, 0.5, 0.7,$  and  $0.9$ .

conditions and then decreases to a state of critical outflow. Once attained, the solution further evolves with critical conditions at the outflow towards the long-time similarity form governed by (14) and (15) with  $F(1) = 1$ . However, importantly, the transition to criticality at the outflow takes a long time.

Examples of the similarity solution for  $0 < r_i < 1$  are plotted in Fig. 6. They were computed by integrating (14) and (15) from  $r = 1 - \delta$  ( $\delta \ll 1$ ) using

$$\frac{V(1 - \delta)}{V_0} = 1 - \left( \delta \frac{2(1 - V_0)}{3V_0} \right)^{1/2} + \dots \quad \text{and} \quad F(1 - \delta) = 1 - \left( \delta \frac{3(1 - V_0)}{2V_0} \right)^{1/2} + \dots, \quad (17)$$

where  $\delta$  is picked sufficiently small that the computed solution does not depend upon it. The integration is halted when  $V(r)$  vanishes and by iteratively varying  $V_0$  we can find the self-similar solution for each  $r_i$ . The dependence of the outflow velocity,  $V_0$ , upon  $r_i$  is analyzed in the Appendix, notably demonstrating that the result for 2D flows is attained when  $|1 - r_i| \ll 1$  (cf. [15]).

#### D. Effects of the initial conditions on the outflow Froude number

The numerical computations demonstrate that for a cylindrical reservoir ( $r_i = 0$ ) the Froude number at the outflow,  $F_o$ , asymptotes to a constant value at late times and that the outflow is supercritical. Furthermore, we have shown that flow with any supercritical outflow (with Froude number  $F_o > 1$ ) is an admissible self-similar state. In this subsection we demonstrate that this asymptotic value of  $F_o$  is dependent on the initial conditions and is established through the dynamics that occur at relatively early times. To illustrate this effect, rather than imposing an initially uniform depth of fluid throughout the reservoir, we choose the initial condition

$$h(r, 0) = 1 + (h_i - 1)\left(1 - \frac{3}{2}r\right), \quad (18)$$

where  $0 \leq h_i \leq 3$  is a constant that parametrizes a family of initial conditions that have the same total volume of fluid (and  $h_i = 1$  corresponds to the initial condition investigated in Sec. III). We numerically integrate the system of governing equations (1)–(4) subject to (18) and evaluate the Froude number at the outflow. In Fig. 7 we plot the outflow Froude number as a function of  $h_i$  at two relatively late times in the evolution ( $t = 30$  and  $50$ ), showing that the flow dynamics evolve to a state in which the Froude number remains constant in time. However, this asymptotic Froude number varies quite significantly with  $h_i$ , and notably there is a local minimum when  $h_i \approx 2.38$ . For this family of initial conditions, (18), the earliest stages of the motion include a rarefaction fan centered at the outflow ( $r = 1$ ). The fan connects continuously to the initial evolution in the rest of the reservoir. We find numerically that when  $h_i \approx 2.38$ , the  $\beta$  characteristic from the rearmost edge of the fan is the slowest to leave the domain; for smaller values of  $h_i$ , the  $\beta$  characteristic is reflected from the back of the domain ( $r = 0$ ), while for larger values, the direction  $\beta$  characteristic turns

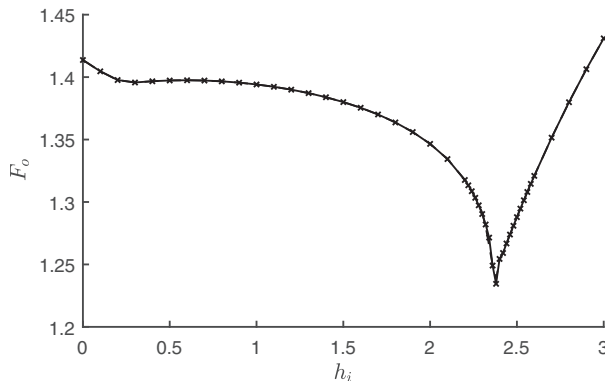


FIG. 7. Froude number at the outflow as a function of  $h_i$  evaluated at  $t = 50$  (solid line, crosses) and  $t = 30$  (dashed line). Note that these curves are virtually indistinguishable.

around sooner and propagates out of the domain. Naturally our results for the temporal variation of the outflow Froude number and its asymptotic value are strongly dependent upon the initial conditions and here we have investigated only a simple class of functions. However, this illustrates that the asymptotic value of the Froude number depends upon the variation at relatively early times. Thus the similarity solution to which the system evolves at much later times is rather unlike other similarity states for gravity currents that become independent of the precise initial conditions.

#### IV. LOCK-RELEASE GRAVITY CURRENTS

We now analyze the development of a gravity current, initiated from lock-release conditions to flow radially, modeled using the shallow water equations, (1) and (2). The motion is subject to the dynamic condition at its moving front, (5), and we analyze the development of the flow for various values of the imposed, constant Froude number at the front,  $Fr$ .

At very early times following initiation and before the motion is affected by the radial geometry and its finite extent, the flow corresponds to a simple-wave centered on  $r = 1$ , ahead of which the depth and velocity are constant [9,14]. Writing  $y = (r - 1)/t$  as in Sec. III and the dependent variables as  $h = h_0(y) + th_1(y) + \dots$  and  $u = u_0(y) + tu_1(y) + \dots$ , the leading-order solution is given by

$$h_0 = \begin{cases} 1, & y < -1, \\ \frac{1}{9}(2 - y)^2, & -1 < y < y_{c0}, \\ \frac{1}{9}(2 - y_{c0})^2, & y_{c0} < y < y_{N0}, \end{cases} \quad \text{and} \quad u_0 = \begin{cases} 0, & y < -1, \\ \frac{2}{3}(1 + y), & -1 < y < y_{c0}, \\ \frac{2}{3}(1 + y_{c0}), & y_{c0} < y < y_{N0}, \end{cases} \quad (19)$$

where  $y_{c0} = 2(Fr - 1)/(Fr + 2)$  and  $y_{N0} = 2Fr/(Fr + 2)$ . This leading-order solution includes a fan of  $\beta$  characteristics that are straight lines, emanating from  $r = 1$ , ahead of which there is a region in which  $h$  and  $u$  are constants. On the lead  $\beta$  characteristic, the invariant takes the value  $\beta = \beta_{c0} = 2(Fr - 2)/(2 + Fr)$ . Including the  $O(t)$  perturbations to these fields leads to the turnaround of initially rearward-propagating  $\beta$  characteristics as the fluid in the lock becomes supercritical. The perturbation is given by (7) and the lead characteristic by (8) with  $\beta_0 = \beta_{c0}$ . This may be matched to a perturbation within the ‘constant’ region at the front of the flow, in which the dependent fields are linear functions of  $y$ , and to the perturbed front position, which is decelerated. The upshot is that the fan region generated by the release develops supercritical flow, whereas the front is retarded somewhat by radial spreading. Although at early times the fields remain continuous, eventually it is no longer possible to continuously match the supercritical fluid from the lock release to the less rapidly moving fluid at the front and a shock forms (see Figs. 8 and 9 for  $Fr = \sqrt{2}$  and Fig. 10 for

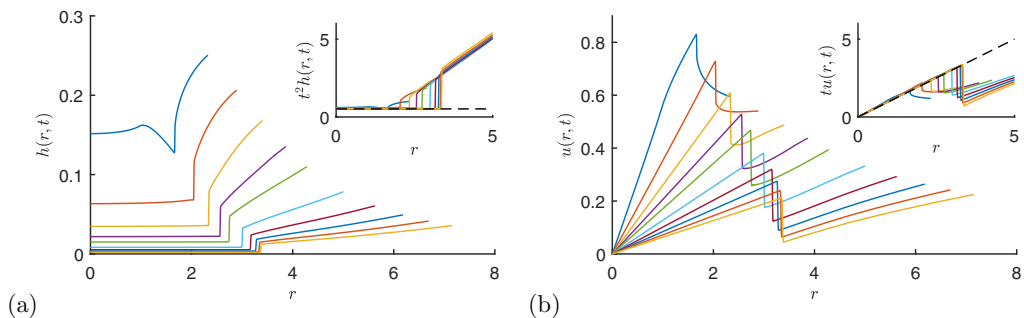


FIG. 8. (a) Height and (b) velocity fields as functions of the radial distance at  $t = 2, 3, 4, 5, 6, 8, 10, 12, 14,$  and  $16$  for  $\text{Fr} = \sqrt{2}$ . Inset: The similarity solution, (16), with  $F_o = 1.39$  (dashed lines) is also included.

$\text{Fr} = 2$ ). This shock is entirely associated with the onset of supercriticality within the lock due to the radial geometry; it does not occur for 2D releases (see [14]). Although the shock formation has been reported before in numerical simulations of the shallow water equations (see, for example, [9, 12]), it has not previously been explained in terms of the onset of supercriticality due to lock-release initial conditions.

Once the shock is formed it propagates forwards initially, while the fluid behind it evolves to the self-similar state reported above in the study of free drainage [given by (16) with  $F_o = 1.39$ ], as shown in Figs. 8 and 10. Downstream of the shock, the fields are strongly affected by the front condition, here expressed through the magnitude of the Froude number at the front,  $\text{Fr}$ , and as shown below, we find a difference in the behavior depending on whether  $\text{Fr} \leq \sqrt{2}$  or  $\text{Fr} > \sqrt{2}$ .

### A. Gravity currents with $\text{Fr} \leq \sqrt{2}$

When  $\text{Fr} \leq \sqrt{2}$ , the depth of fluid upstream of the internal shock eventually becomes so thin relative to the downstream depth that the shock reverses its direction of motion and heads towards the origin. There are instances in which the fluid velocity just downstream of the shock is directed inwards rather than outwards. As it approaches the origin, the shock is amplified due to radial convergence. The shock is then reflected from the origin and propagates forwards, moving faster than the local fluid velocity, and reaches the front, before again being reflected towards the origin. This pattern of shock reflections superimposed upon a bulk flow is similar to the reflections of continuous waves in 2D gravity currents [14] and draining flows from partially breached reservoirs [28].

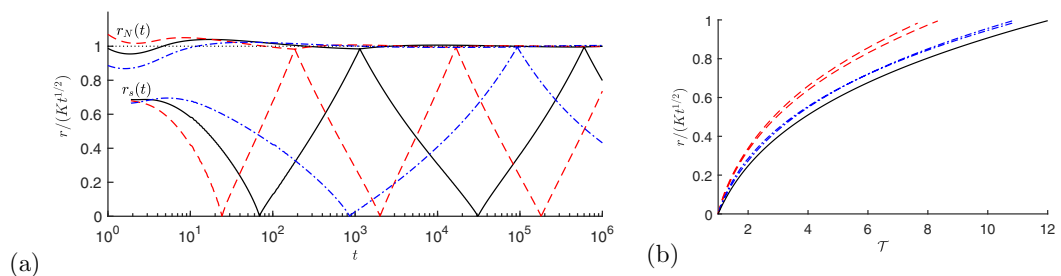


FIG. 9. (a) The position of the front of the current,  $r_N(t)$ , and the trajectory of shock,  $r_s(t)$ , as functions of the time for  $\text{Fr} = 1$  (dashed red lines),  $\text{Fr} = 2^{1/4}$  (solid black lines), and  $\text{Fr} = 2^{1/2}$  (dot-dashed blue lines). (b) The positions of the outward (dashed red lines)- and inward (dot-dashed blue line)-propagating shocks and the characteristic curves from the similarity solution, (20) as functions of  $\mathcal{T}$  (solid black line).

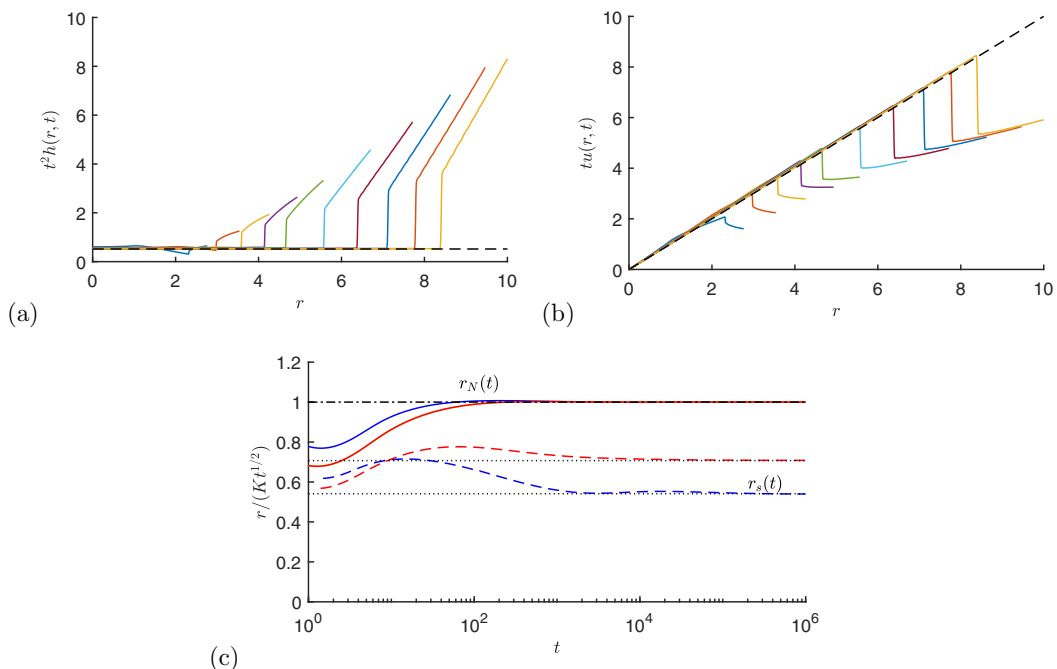


FIG. 10. (a) Rescaled height,  $t^2 h(r, t)$ , and (b) rescaled velocity,  $tu(r, t)$ , fields as functions of the radial distance at  $t = 2, 3, 4, 5, 6, 8, 10, 12, 14,$  and  $16$  for  $\text{Fr} = 2$  (solid lines). Also plotted is the supercritical similarity solution, (16), with  $F_o = 1.39$  (dashed line). (c) Position of the front,  $r_N(t)$  (solid lines), and the shock,  $r_s(t)$  (dashed lines), for  $\text{Fr} = 2^{3/4}$  (blue) and  $\text{Fr} = 2$  (red). The asymptotic state,  $r = r_b$ , is also plotted (dotted black line).

Our computations were able to track this motion over several reflected cycles, during which the amplitude of the shock, here measured by the relative increase in depth, became smaller and its speed of propagation slower. We plot in Fig. 9 the position of the shock,  $r_s(t)$ , for three values of  $\text{Fr} \leq \sqrt{2}$ . In each case, we observe the same pattern of successive reflections between the origin and the front, though the speed of the shock is strongly dependent on  $\text{Fr}$ .

After very long times following release the overall motion approaches the similarity solution [12,17] for which  $\eta = r/(Kt^{1/2})$  and

$$u = \frac{K}{2t^{1/2}}\eta \quad \text{and} \quad h = \frac{K^2}{8t} \left( \eta^2 + \frac{2}{\text{Fr}^2} - 1 \right), \quad (20)$$

where  $K^4 = 16\text{Fr}^2/(4 - \text{Fr}^2)$  provided  $\text{Fr} \leq \sqrt{2}$ . The position of the front,  $r_N(t)$ , corresponds to  $\eta = 1$  and our numerical simulations show convergence to this state (Fig. 9). We emphasize that the similarity solution, (20), is concerned with the propagating gravity current, while the similarity solution constructed in Sec. III C is concerned with the domain of the lock. As shown in Fig. 8, both solutions can coexist in certain circumstances. At later times, the motion of the shock is ‘superimposed’ upon the self-similar solution for gravity currents, (20). As the amplitude of the shock diminishes, its velocity approaches the characteristic velocity  $u + h^{1/2}$  when it is propagating forwards and  $u - h^{1/2}$  when it is propagating rearwards. Using the similarity solution, (20), we may calculate the trajectory of  $\alpha$  characteristics propagating from the rear to the front of the current and  $\beta$  characteristics propagating from the front to the rear. These trajectories, determined by integrating

$dr_c/dt = u \pm h^{1/2}$ , are given by

$$r_c = Kt^{1/2} \left( \frac{2}{\text{Fr}^2} - 1 \right)^{1/2} \sinh \left( \frac{\pm 1}{\sqrt{8}} \log \left( \frac{t}{t_0} \right) \right), \quad (21)$$

where  $r_c(t_0) = 0$ . We compare this result for both inward- and outward-propagating shocks with the numerically computed trajectories [Fig. 9(b)]. In this figure we plot the scaled radial shock position,  $r_c/(Kt^{1/2})$ , as a function of  $\mathcal{T} = (t/t_0)^{\pm 1}$  with  $\text{Fr} = 1$ , which features the largest number of reflections in our simulated cases. We note that the evolution approaches this limiting case of moving at the characteristic velocity but that the shock is still somewhat faster moving when propagating forwards. This arises because the amplitude of the shock is very considerably amplified local to the origin due to radial convergence, and this leads to more rapid movement of the shock away from the origin. Reflections from the front that subsequently propagate inwards are not amplified in the same way.

### B. Gravity currents with $\text{Fr} > \sqrt{2}$

When the current is significantly denser than the surroundings (i.e., it is non-Boussinesq),  $\text{Fr} > \sqrt{2}$  and the evolution of the interior shock is somewhat different, as is the similarity solution to which the dynamics tend at long times after release. For these values of  $\text{Fr}$ , we note from (20) that  $h = 0$  at  $\eta = \eta_b = (\text{Fr}^2 - 2)^{1/2}/\text{Fr}$  and the similarity solution enforces the absence of fluid in a region around the origin ( $0 < r < r_b(t) \equiv K\eta_b t^{1/2}$ ); thus  $K = 2^{1/2}\text{Fr}$  [29]. The shock that forms at relatively early times as a consequence of the generation of supercritical flow does not reflect between the origin and the front of the fluid. Instead it tends to  $r_b(t)$  (Fig. 10). Upstream of the shock the fluid remains in the self-similar, supercritical flow state determined by (16) with  $F_o = 1.39$ , as shown in Fig. 10. Downstream of the shock it evolves progressively towards the similarity solution given, (20), and the mismatch between these solutions is confined to a narrow region adjacent to the shock.

At late times ( $t \gg 1$ ), the depth of the fluid layer downstream of the shock far exceeds the depth upstream, which has thinned rapidly and transitioned to the supercritical self-similar state, (16). In this regime, the leading-order balance of the momentum flux across the shock requires that

$$\left( u(r_s^-, t) - \frac{dr_s}{dt} \right)^2 h(r_s^-, t) = \frac{h(r_s^+, t)^2}{2}, \quad (22)$$

where the  $-$  and  $+$  superscripts denote evaluation of the functions upstream and downstream of the shock, respectively. Using (16) and (20) to determine the leading-order expressions for the dependent variables upstream and downstream of the shock, respectively, we therefore deduce that

$$r_s(t) = r_b(t) + \frac{1}{2^{3/2}F_o} + \dots \quad (23)$$

Thus the relative amplitude of the perturbation to the similarity solution, (20), decays as  $O(t^{-1/2})$  when  $t \gg 1$ , which differs from the linearized perturbations found for gravity currents with  $1 \leq \text{Fr} \leq \sqrt{2}$  that extend back to the origin. Furthermore, it may not be accounted for by the inclusion of a temporal offset in the similarity solution either upstream, (16), or downstream, (20), of the shock, which would lead to corrections of  $O(t^{-1})$ . We also deduce from (16) and (20) that the velocity drops across the shock by a factor of 2, from  $r_s/t$  to  $r_s/(2t)$ .

## V. CONCLUSIONS

In this study we have demonstrated the surprising result that from lock-release initial conditions, radial flows become supercritical in a region close to the symmetry axis. This transition occurs for both Boussinesq and non-Boussinesq releases and is solely due to the radial geometry; it

does not occur for two-dimensional flows. The development of supercritical motion has important consequences.

First, for free draining over an edge, the outflow is not under critical conditions and the problem is overspecified by imposing that the edge Froude number,  $F_o$ , is unity as the boundary condition. Instead, the Froude number at the outflow increases from a unit value during an initial period and, for releases from a cylindrical reservoir, attains a constant value that persists through the rest of the motion. The flow also evolves to a self-similar state with a supercritical outflow. For an annular reservoir, the dynamics are more complicated. The Froude number,  $F_o$ , still initially increases, but then over a potentially long period, dependent on the inner radius of the annulus, it decays and eventually the outflow becomes critically controlled. The numerical implementation of the drainage boundary condition therefore requires care to avoid overspecification and to maintain the appropriate form consistent with the interior dynamics.

The second consequence is for radial gravity currents. In this scenario the onset of supercriticality in the region close to the symmetry axis eventually leads to the development of an internal jump to connect the rapid upstream motion to the more tranquil state at the front. The shock emerges at relatively early dimensionless times (e.g., for  $Fr = \sqrt{2}$  we first detect it numerically at  $t \approx 1.9$ ). Upstream of the shock, the flow becomes identical to the similarity solution for unsteady radial drainage—namely,  $u = r/t$  and  $h = 1/(F_o^2 t^2)$ —whereas downstream it evolves to match the frontal boundary condition, progressively evolving to the self-similar state for radial gravity currents, (20). Interestingly, the velocity decreases across the shock from one state of linear variation with radial distance ( $u = r/t$ ) to another [ $u = r/(2t)$ ]. The presence of the shock affects the progressive evolution of the gravity current towards the self-similar state. If  $Fr < \sqrt{2}$ , then the initially forward-propagating shock is reversed and successively reflects between the origin and the front of the flow. Its amplitude weakens and asymptotically it moves at the speed of the forward- and rearward-moving characteristics. Conversely, if  $Fr > \sqrt{2}$ , then the direction of movement of the shock does not reverse, and it forms the connection between the thin layer of fluid upstream and the bulk of the fluid moving outwards in an annulus. The shock amplitude also decreases, but at a rate that is not captured by current linear stability analyses of the long term similarity solutions.

This study has demonstrated that the radial geometry influences the dynamics of density-driven flows, generating effects that steer the long-term development of the motion. We anticipate similar effects in related model systems, such as the intrusion of a volume of fluid through a stratified ambient [30–32]. We advocate the use of numerical methods that are designed to impose (and not overspecify) the boundary conditions. Finally, we comment that it would be invaluable to test these theoretical predictions against laboratory experiments; we cannot do so currently due to the lack of data. There are experimental challenges in conducting laboratory-scale investigations in which the fluid motion remains inviscid over relatively long radial length scales, although this is the natural regime for many field-scale releases [2,3,5,6]. Furthermore there are challenges in measuring the velocity and density fields (e.g., [31]). The verification of critical flow behavior and of the evolution of internal jumps requires high-resolution data guided by a precise theory. We hope that the present investigation will motivate such an experimental program.

#### ACKNOWLEDGMENT

E.W.G.S. acknowledges the financial support of the EPSRC, UK (Grant No. EP/M506473/1).

#### APPENDIX: SIMILARITY SOLUTION FOR FREE DRAINING FROM AN ANNULAR LOCK

This Appendix analyzes the similarity solution for free draining from an annular lock, for which it was demonstrated that the motion becomes critical at the outflow at long times after release (Sec. III C). The governing equations for this new class of similarity solutions are given by (14) and (15), subject to criticality at the outflow,  $F(1) = 1$ , and no flow at the back wall,  $V(r_i) = 0$ .

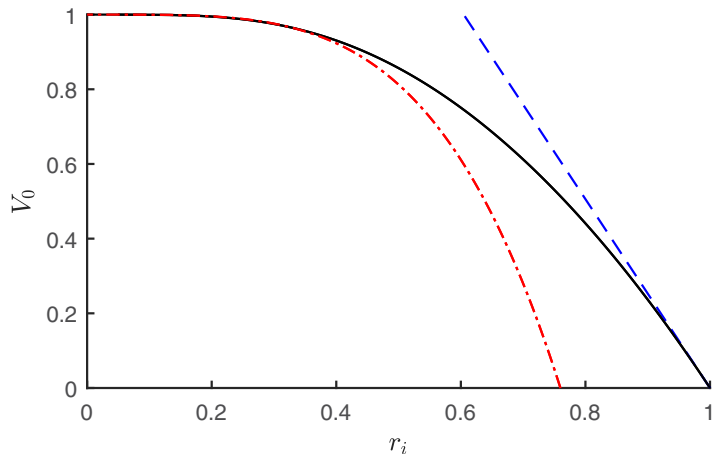


FIG. 11. Velocity of the similarity solution at the outflow,  $V_0$ , as a function of the inner annular radius,  $r_i$ , showing numerical computations (solid black line) and asymptotic solutions for  $r_i \ll 1$  (dot-dashed red line) and  $1 - r_i \ll 1$  (dashed blue line).

Here we analyze the relationship between the velocity at the outflow,  $V(1) = V_0$ , and the inner radius,  $r_i$ .

Numerically integrating the governing equations using the shooting technique described in Sec. III C yields the results plotted in Fig. 11. We now examine this relation using asymptotic analysis in the regimes of a small ( $r_i \ll 1$ ) or large ( $|1 - r_i| \ll 1$ ) inner radius.

First, it is convenient to write

$$\frac{dV}{dF} = -\frac{2V(V-1)(F^2-2)}{F(F^2(V+1)+2V-4)}. \quad (\text{A1})$$

When  $|1 - r_i| \ll 1$ , because  $V(r_i) = 0$ , we anticipate that  $V_0 \ll 1$ . Thus we can linearize (A1) and apply the boundary conditions at  $r = 1$  to find that

$$\frac{V}{V_0} = F \left( \frac{4 - F^2}{3} \right)^{1/2}. \quad (\text{A2})$$

Then substituting for  $V(r)$  in (15) and integrating, we find that

$$\int_0^1 \frac{F^2 - 1}{(4 - F^2)^{1/2}} dF = -\frac{3^{1/2}}{2V_0} \log(r_i). \quad (\text{A3})$$

Since  $V_0 \ll 1$ , this requires that  $|1 - r_i| \ll 1$  and so we determine that

$$V_0 = \frac{3\sqrt{3}}{3\sqrt{3} - \pi} (1 - r_i) + \dots. \quad (\text{A4})$$

This result, (A4), is identical to that derived by [15] for 2D free drainage, as it must be, because the effects of polar geometry are negligible when  $|1 - r_i| \ll 1$ .

Conversely, we analyze the case when  $r_i \ll 1$ , for which we write  $V_0 = 1 - \epsilon$  ( $0 < \epsilon \ll 1$ ). By substituting  $V = 1 - \epsilon U$  and  $F = 1 - G$  into (A1) we find that, to leading order,

$$\frac{dU}{dG} = \frac{2U(-1 - 2G + G^2)}{(1 - G)(-4G + 2G^2 - \epsilon U(3 - 2G + G^2))}. \quad (\text{A5})$$

When  $G = O(1)$  we may further linearize the denominator and integrate to find that

$$U = B \frac{(G(2-G))^{1/2}}{(1-G)^2}, \quad (\text{A6})$$

where  $B$  is constant. When  $G = O(\epsilon)$ , we substitute  $G = \epsilon \hat{g}$  into (A5), integrate, and apply the boundary condition that  $U = 1$  at  $\hat{g} = 0$  to deduce that

$$U = \frac{1}{2} \left( 1 + \left( 1 + \frac{8\hat{g}}{3} \right)^{1/2} \right). \quad (\text{A7})$$

Matching (A6) and (A7) determines  $B = (3\epsilon)^{-1/2}$ . We may also determine the dependence on  $r$ : substituting into (14), integrating, and matching, we deduce that  $G = 1 - r$  and thus

$$V = 1 - \left( \frac{\epsilon}{3} \right)^{1/2} \frac{(1-r^2)^{1/2}}{r^2}. \quad (\text{A8})$$

This expression becomes nonasymptotic when  $r = O(\epsilon^{1/4})$  and  $F = O(\epsilon^{1/4})$ , while  $V = O(1)$ . Writing  $\xi = r/\epsilon^{1/4}$  and substituting into (14), we find that, to leading order,

$$V = 1 - \frac{\xi_i^2}{\xi^2}, \quad (\text{A9})$$

where  $\xi_i = r_i/\epsilon^{1/4}$ . Matching (A9) and (A8) then determines that  $\epsilon = 3r_i^4$ , and consequently,

$$V_0 = 1 - 3r_i^4 \quad \text{when} \quad r_i \ll 1. \quad (\text{A10})$$

We superimpose both of these asymptotic expressions, (A10) and (A4), on the plotted, numerically computed result and find that they accurately predict the results in their relevant regimes (see Fig. 11).

- 
- [1] J. E. Simpson, *Gravity Currents in the Environment and the Laboratory* (Cambridge University Press, Cambridge, UK, 1997).
- [2] R. G. Picknett, Dispersion of dense gas puffs released in the atmosphere at ground level, *Atmos. Environ.* **15**, 509 (1981).
- [3] J. A. Fay and D. A. Ranck, Comparison of experiments on dense gas cloud dispersion, *Atmos. Environ.* **17**, 239 (1983).
- [4] R. K. S. Hankin and R. E. Britter, TWODEE: The Health and Safety Laboratory's shallow layer model for heavy gas dispersion. Part 1. Mathematical basis and physical assumptions, *J. Hazard. Mater.* **66**, 211 (1999).
- [5] R. S. J. Sparks, J. G. Moore, and C. J. Rice, The initial giant umbrella cloud of the May 18, 1980 explosive eruption of Mount St. Helens, *J. Volcanol. Geotherm. Res.* **28**, 257 (1986).
- [6] A. W. Woods and J. Kienle, The dynamics and thermodynamics of volcanic clouds: Theory and observations from the April 15 and April 21, 1990 eruptions of Redoubt Volcano, Alaska, *J. Volcanol. Geotherm. Res.* **62**, 273 (1994).
- [7] C. G. Johnson, A. J. Hogg, H. E. Huppert, R. S. J. Sparks, J. C. Phillips, A. C. Slim, and M. J. Woodhouse, Modelling intrusions through quiescent and moving ambients, *J. Fluid Mech.* **771**, 370 (2015).
- [8] M. A. Hallworth, H. E. Huppert, and M. Ungarish, Axisymmetric gravity currents in a rotating system: Experimental and numerical investigations, *J. Fluid Mech.* **447**, 1 (2001).
- [9] M. Ungarish, *An Introduction to Gravity Currents and Intrusions* (CRC Press, Boca Raton, FL, 2009).
- [10] M. I. Cantero, S. Balachandar, and M. H. Garcia, High-resolution simulations of cylindrical density currents, *J. Fluid Mech.* **590**, 437 (2007).
- [11] M. Ungarish, Axisymmetric gravity current at high Reynolds number: On the quality of shallow-water modeling of experimental observations, *Phys. Fluids* **19**, 036602 (2007).

- [12] R. E. Grundy and J. W. Rottman, The approach to self-similarity of the solutions representing gravity current releases, *J. Fluid Mech.* **156**, 39 (1985).
- [13] J. S. Mathunjwa and A. J. Hogg, Stability of gravity currents generated by finite volume releases, *J. Fluid Mech.* **562**, 261 (2006).
- [14] A. J. Hogg, Lock-release gravity currents and dam-break flows, *J. Fluid Mech.* **569**, 61 (2006).
- [15] M. Momen, Z. Zheng, E. Bou-Zeid, and H. A. Stone, Inertial gravity currents produced by fluid drainage from an edge, *J. Fluid Mech.* **827**, 640 (2017).
- [16] M. Ungarish, L. Zhu, and H. A. Stone, Inertial gravity current produced by the drainage of a cylindrical reservoir from an outer or inner edge, *J. Fluid Mech.* **874**, 185 (2019).
- [17] D. P. Hoult, Oil spreading on the sea, *Annu. Rev. Fluid Mech.* **4**, 341 (1972).
- [18] M. Ungarish, C. G. Johnson, and A. J. Hogg, A novel hybrid model for the motion of sustained axisymmetric gravity currents and intrusions, *Eur. J. Mech. B/Fluids* **49**, 108 (2015).
- [19] M. Ungarish, C. G. Johnson, and A. J. Hogg, Sustained axisymmetric intrusions in a rotating system, *Eur. J. Fluid Mech. B* **56**, 110 (2016).
- [20] T. B. Benjamin, Gravity currents and related phenomena, *J. Fluid Mech.* **31**, 209 (1968).
- [21] M. Ungarish and A. J. Hogg, Models of internal jumps and the fronts of gravity currents: Unifying two-layer theories and deriving new results, *J. Fluid Mech.* **846**, 654 (2018).
- [22] H. E. Huppert and J. E. Simpson, The slumping of gravity currents, *J. Fluid Mech.* **99**, 785 (1980).
- [23] E. W. G. Skevington, The implementation of a broad class of boundary conditions for non-linear hyperbolic systems, [arXiv:2106.11262](https://arxiv.org/abs/2106.11262).
- [24] A. Kurganov, S. Noelle, and G. Petrova, Semi-discrete central-upwind schemes for hyperbolic conservation laws and Hamilton-Jacobi equations, *SIAM J. Sci. Comput.* **23**, 707 (2001).
- [25] E. W. G. Skevington, A well-balanced reconstruction with bounded velocities for the shallow water equations by convex combination, [arXiv:2106.11273](https://arxiv.org/abs/2106.11273).
- [26] E. W. G. Skevington, A well balanced reconstruction with bounded velocities and low-oscillation slow shocks for the shallow water equations, [arXiv:2106.11256](https://arxiv.org/abs/2106.11256).
- [27] A. Ritter, Die Fortpflanzung der Wasserwellen, *Z. Vereines Deutsch. Ingen.* **36**, 947 (1892).
- [28] E. W. G. Skevington and A. J. Hogg, Unsteady draining of reservoirs over weirs and through constrictions, *J. Fluid Mech.* **882**, A9 (2020).
- [29] J. Gratton and C. Vigo, Self-similar gravity currents with variable inflow revisited: Plane currents, *J. Fluid Mech.* **258**, 77 (1994).
- [30] M. Ungarish and T. Zemach, On axisymmetric intrusive gravity currents in a stratified ambient—Shallow-water theory and numerical results, *Eur. J. Mech. B/Fluids* **26**, 220 (2007).
- [31] A. M. Holdsworth, S. Decamp, and B. R. Sutherland, The axisymmetric collapse of a mixed patch and internal wave generation in uniformly stratified fluid, *Phys. Fluids* **22**, 106602 (2010).
- [32] A. M. Holdsworth, K. J. Barrett, and B. R. Sutherland, Axisymmetric intrusions in two-layer and uniformly stratified environments with and without rotation, *Phys. Fluids* **24**, 036603 (2012).